Biosensors and Bioelectronics 142 (2019) 111503

Contents lists available at ScienceDirect

Biosensors and Bioelectronics

journal homepage: www.elsevier.com/locate/bios

An ultrasensitive electrochemical aptasensor for the determination of tumor exosomes based on click chemistry

Yu An, Tongyu Jin, Yuyuan Zhu, Fan Zhang*, Pingang He

School of Chemistry and Molecular Engineering, East China Normal University, 500 Dongchuan Road, Shanghai, 200241, PR China

ARTICLE INFO

Keywords:
Exosomes
Alkynyl-4-ONE
Click chemistry
Aptamer
Electrochemical aptasensor

ABSTRACT

Exosomes, lipid bilayer membrane vesicles, can guide various pathological and physiological processes. However, reliable, convenient and sensitive methods for exosome determination for early cancer diagnosis are still technically challenging. Herein, an electrochemical aptasensor based on click chemistry and the DNA hybridization chain reaction (HCR) for signal amplification has been developed for the ultrasensitive detection of tumor exosomes. CD63 aptamer was first immobilized on a glassy carbon electrode for capturing exosomes, and 4-oxo-2-nonenal alkyne (alkynyl-4-ONE) molecules, functionalized lipid electrophiles, were conjugated to the exosomes via the reaction of amino and aldehyde groups. Azide-labeled DNA probe as an anchor was then connected to the exosomes by copper (I)-catalyzed click chemistry. Signal amplification was achieved by HCR, and the numerous linked horseradish peroxidase (HRP) molecules could catalyze the reaction of o-phenylenediamine (OPD) and H_2O_2. The concentration of exosomes could be quantified by monitoring the electrochemical reduction current of 2,3-diaminophenazine (DAP). Under the optimal conditions, this method allowed the sensitive detection of exosomes in the range of 1.12×10^2 to 1.12×10^8 particles/μL with a limit of detection (LOD) of 96 particles/μL. Furthermore, the present assay enabled sensitive and accurate quantification of exosomes in human serum, and it has high potential for exosome analysis in clinical samples.

1. Introduction

Exosomes, lipid bilayer membrane vesicles with a diameter of 30–150 nm, are secreted by numerous mammalian cell types, and they are widely found in a variety of body fluids, such as blood, urine, tears, saliva, breast milk, cerebrospinal fluid and so on (Conlan et al., 2017). Since exosomes were first coined by Trams's group in the early 1980s, the relationship between exosomes and tumor has received considerable attention (Zhao et al., 2015). After tumorigenesis, exosomes have important changes in the number and protein expression. Compared to healthy controls, tumor patients have more exosomes in their peripheral blood (Suchorska and Lach, 2016), and the exosomes express tumor-specific proteins with the occurrence of tumor (Azmi et al., 2013; Shao et al., 2018). Therefore, exosomes can serve as a new noninvasive biomarker for the diagnosis of cancers.

To date, the analysis of the number of exosomes has been realized by various methods. Common direct particle counting methods include nanoparticle tracking analysis (NTA) and flow cytometry. NTA is a powerful technique to allow the visualization and calculation of individual exosomes. However, the determination is easily interfered by similarly sized lipoproteins and protein aggregates (Vestad et al., 2017). Flow cytometry can achieve high-throughput and quantitative determination of exosomes, but some in small size (< 100 nm) would be missed, decreasing the accuracy of the measurement (Pospichalova et al., 2015). The methods based on the specific recognition of proteins on the surface of exosomes include enzyme-linked immunosorbent assays (ELISA), fluorescent determination and electrochemical determination. ELISA is commercially available, but a relatively large number of exosomes are required. Additionally, the detection limit is approximately 10^7 particles/μL (Jeong et al., 2016). Recently, fluorescent and electrochemical platforms have been developed for exosome analysis with high sensitivity (Chen et al., 2018; Xia et al., 2017). These approaches employ antigens or aptamers to recognize the special proteins on the surface of exosomes (Tian et al., 2018a,b; Boriachek et al., 2017). However, these proteins are not homogeneously expressed on different subpopulations of exosomes from the same cellular origin (Picciolini et al., 2018; Zhang et al., 2018), and thus, some exosome subpopulations would be missed in the measurement. Therefore, there is an urgent need to recognize exosomes in a nonspecific way for more accurate quantitative analysis. Ye et al. recently reported a novel strategy via cholesterol-assisted lipid membrane modification to quantify exosomes. The bivalent-cholesterol-labeled DNA anchors were

* Corresponding author.
E-mail address: fzhang@chem.ecnu.edu.cn (F. Zhang).

https://doi.org/10.1016/j.bios.2019.111503
Received 8 April 2019; Received in revised form 19 June 2019; Accepted 12 July 2019
Available online 13 July 2019
0956-5663/

inserted into the phospholipid membrane by means of non-covalent bonds (He et al., 2017, 2018). Also, some researchers have successfully conjugated fluorescent molecules to exosomes without protein selectivity via a click chemistry reaction.

Click chemistry was first introduced by Barry Sharpless in 1999 and has gained considerable applications in numerous related fields (Moses and Moorhouse, 2007). One of the most popular click chemical reactions is the copper (I)-catalyzed alkyne-azide 1,3-dipolar cycloaddition (CuAAC) reaction with temperate reaction conditions, high reactivity and high efficiency (Liang and Astruc, 2011), and it has been widely used in organic chemical synthesis as well as drug discovery, especially in the modification and functionalization of biomacromolecules (Uttamapinant et al., 2012). The membrane of exosomes is composed of a phospholipid bilayer, which is rich in transmembrane and lipid-bound extracellular proteins. Thus, the membrane surface engineering of exosomes can be implemented by biochemical conjugation. Thus far, several reports have demonstrated that click chemistry could be applied to the protein modification of exosomes. For example, Thomas et al. developed a click chemistry method for the conjugation of azide-fluor 454 ligands to the surface of exosomes by 4-pentynoic acid (Smyth et al., 2014). Xu et al. reported that azide-containing compounds were cocultured with cells to produce azide active sites on the exosomes, followed by the further conjugation of dibenzobicyclooctyne (DBCO) to the surface of exosomes without copper catalysis for intracellular application (Wang et al., 2015). Similarly, Gao et al. used a copper-free azide alkyne cyclo-addition to conjugate functional ligands onto the exosome surface via DBCO for drug delivery (Tian et al., 2018a,b). However, these methods have common disadvantages, including the long time required for the modification of the exosomes and the low modification efficiency, thus increasing the cost of testing and affecting the sensitivity of the detection.

In this work, an electrochemical method based on click chemistry was developed for the determination of tumor exosomes with hybridization chain reaction (HCR) for signal amplification (Scheme 1). Since abundant CD63 proteins were exposed on the surface of exosomes, they could be captured by the CD63 aptamer on the electrode. Different from most of the previous assays based on specific protein recognition, alkynyl-4-ONE, showing high reactivity toward proteins (Aluise et al., 2015; Galligan et al., 2014), was used to modify exosomes derived from MCF-7 cells, followed by the conjugation of an azide-labeled DNA probe as an anchor through a copper (I)-catalyzed click chemistry reaction. With the addition of auxiliary DNA, long self-assembled DNA concatemers were formed by HCR for signal amplification. The numerous linked HRP catalyzed the oxidation of o-phenylenediamine (OPD), and the further reduction current signal was monitored to quantify the exosomes. In this way, the strengths of click chemistry and HCR technology were combined for the accurate and sensitive detection of tumor exosomes, which has potential application in clinical diagnosis.

2. Experimental section

2.1. Characterization of exosomes

The exosomes and exosomes modified with alkynyl-4-ONE were characterized by TEM and biological fast AFM as previously described with modifications (Sharma et al., 2010). Alkynyl-4-ONE was conjugated to the exosomes via the reaction of amino and aldehyde groups. Briefly, 5 μM alkynyl-4-ONE was added to 1.12×10^6 particles/μL exosomes in PBS and allowed to react on a shaker for 1 h at 37 °C. Subsequently, 5 μL of the unmodified and modified exosomes were placed on the carbon-coated copper grid and let the pellets deposited for 20 min in a dry environment, respectively. This was followed by staining with 1% phosphotungstic acid for 10 s. The excess fluid was gently removed by filter paper and the morphology was observed by TEM. Meanwhile, 5 μL of the two samples were dropped on the mica and dried at room temperature for 20 min, respectively, and imaged by AFM.

The proteins in exosomes were analyzed by Western blot as previously described (Jin et al., 2018). MCF-7 cells and exosomes were lysed by RIPA buffer following quantification of the protein concentration by the BCA method. Then, 10 μg of protein was electrophoresed by 10% SDS-PAGE and electrotransferred to a nitrocellulose filter membrane. After being blocked with 5% BSA, the membranes were incubated overnight with the primary antibodies of α-CD63 and α-Alix at 4 °C, and then, the blots were developed with HRP-conjugated rabbit polyclonal secondary antibodies for 1 h at room temperature. Subsequently, a Gel Image System was employed for imaging the protein strips.

The purified exosomes were sized using nanoparticle tracking analysis (NTA). NTA was performed on a Particle Metrix system, and the concentration of exosomes was determined by tracking the Brownian motion of exosomes suspended in PBS.

2.2. Construction of MCH/CD63 aptamer/DenAu/rGO/GCE

The glassy carbon electrode (GCE, 3 mm in diameter) was successively polished to a mirror finish with 0.3 μm and 0.5 μm alumina slurries, followed by the rinsing with ultra-pure water and drying under a nitrogen flow. Then, the electrochemical reduction of graphene oxide (GO) was performed in 0.5 mg/mL GO solution at −0.8 V (vs. Ag/AgCl) for 400 s. After washing the modified electrode with water, a dendritic gold nanostructure (DenAu) was electrochemically deposited on its surface in 2.8 mM $HAuCl_4$ and 0.1 M H_2SO_4 solution at −1.5 V (vs. Ag/AgCl) for 200 s according to the previously reported procedures (Tang et al., 2018), obtaining the fabricated DenAu/rGO/GCE. For the immobilization of CD63 aptamer on the modified electrode, the CD63 aptamer was dissolved in 10 mM Tris-HCl buffer (containing 10 mM TCEP, pH = 7.4) and incubated at 37 °C for 2 h to reduce the disulfide bonds and facilitate the formation of Au-S bonds. Then, 5 μL of CD63 aptamer solution was dropped on the modified electrode, followed by 24 h of incubation at room temperature. The fabricated CD63 aptamer/DenAu/rGO/GCE was washed with PBS buffer (10 mM, pH = 7.4) and further immersed in 2 mM MCH solution (prepared in 10 mM PBS) at 37 °C for 1 h to block the electrode surface and make the aptamer more erect, thus obtaining the MCH/CD63 aptamer/DenAu/rGO/GCE.

2.3. Electrochemical detection

5 μL of diluted exosome solution at the concentration of ~1.12×10^6 particles/μL in 10 mM PBS (pH = 7.4), calibrated by NTA, was cast onto the surface of MCH/CD63 aptamer/DenAu/rGO/GCE and incubated at 37 °C for 1 h. The unbound exosomes were removed by washing with 10 mM PBS (pH = 7.4). Then, 5 μL of alkynyl-4-ONE solution (diluted in 10 mM PBS, pH = 7.4) was added and incubated at 37 °C for 1 h. Click chemical methods were adapted from the previous work (Smyth et al., 2014). In detail, 5 μL of mixed solution in 10 mM PBS (pH = 7.4), containing N_3-DNA at a specified concentration, 1 mM $CuSO_4$ and 1 mM TCEP solution, was dropped on the electrode and incubated at 37 °C for 1 h. Afterwards, 50 μL of 10 μM H1 and 50 μL of 10 μM H2 were mixed, and 5 μL of the above solution was introduced onto the electrode surface for the HCR. 3 h later, following washing with PBS, the electrode was coated with 5 μL of streptavidin-HRP (5 μg/mL) in 10 mM PBS for 30 min at room temperature and then rinsed to be used for electrochemical detection.

The DPV measurements were performed in the HAc/NaAc buffer solution containing 2 mM OPD and 4 mM H_2O_2 using a conventional three-electrode system with a glassy carbon electrode as the working electrode, Ag/AgCl electrode as the reference electrode and platinum wire as the auxiliary electrode. The current signals were recorded 60 s after the HRP catalyzed reaction reached steady state within the range from −0.6 V to −0.2 V. The pulse amplitude, pulse width and pulse

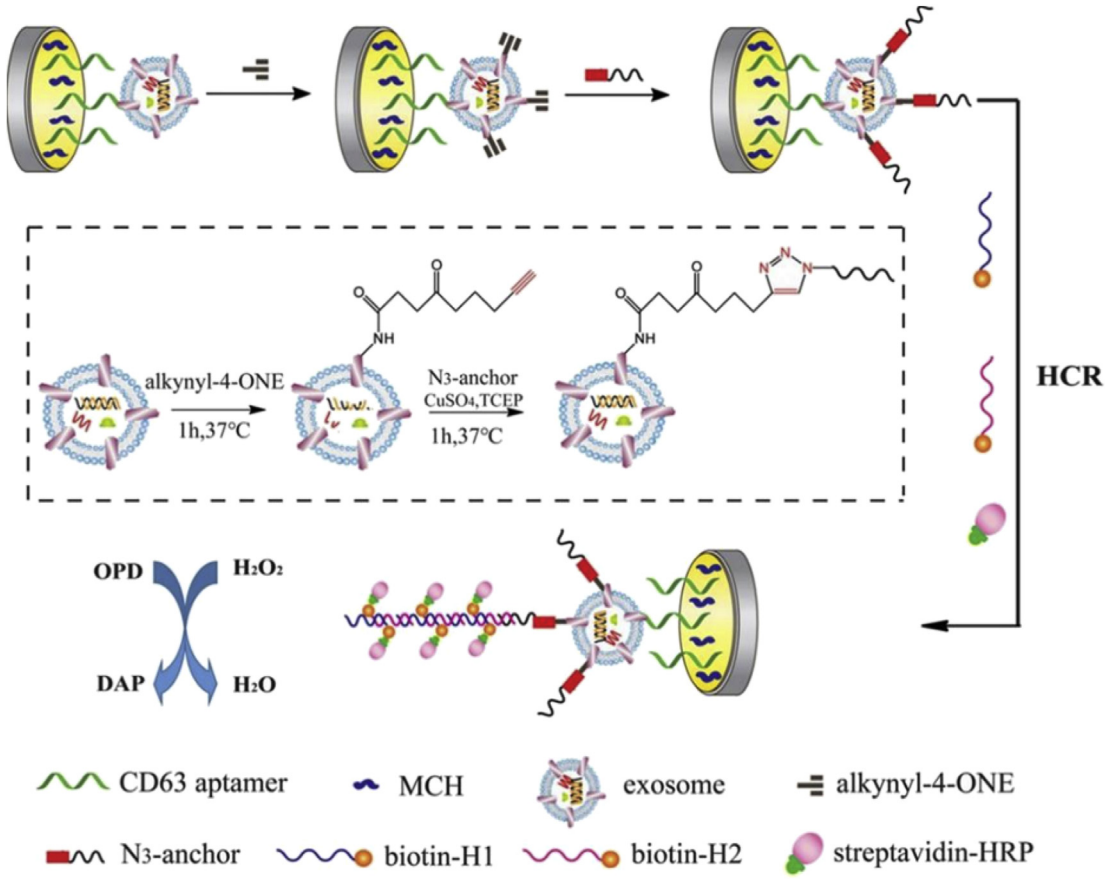

Scheme 1. Schematic illustration of the electrochemical aptasensor for exosome detection based on click chemistry and HCR for signal amplification.

period of DPV were 50 mV, 50 ms, and 0.2 s, respectively. The cyclic voltammetry (CV) and electrochemical impedance measurements (EIS) were operated in 5 mM $[Fe(CN)_6]^{3-/4-}$ solution containing 0.1 M KCl to characterize each immobilization step.

2.4. Detection of exosomes in human serum

The human serum samples of breast cancer patient and healthy individual were obtained from Shanghai Ruijin Hospital. Exosomes were isolated from the human serum using ExoQuick Exosome Isolation Kit according to manufacturer's instructions. Briefly, the serum samples were centrifuged at 3000 g for 15 min to remove the cell debris. The supernatant was collected and added to the isolation reagent at a ratio of 4:1. The samples were incubated at 4 °C for 1 h, followed by centrifugation at 1500 *g* for 30 min. The obtained final exosome pellets were resuspended in 500 μL of PBS and stored at −80 °C until use. The detection procedures for exosomes in serum was consistent with the process of detecting exosomes in cell culture supernatant.

3. Results and discussion

3.1. Characterization of exosomes

The TEM image was used to reveal the morphology of the exosomes. Clearly, these exosomes exhibited a typical cup shape appearance with a diameter of 50–100 nm (Fig. 1A) (Raposo and Stoorvogel, 2013). Fig. 1C shows the results of Western blot analysis, indicating that CD63 and Alix protein, the exosome biomarkers, were enriched in the exosomes (Mathivanan and Simpson, 2009). NTA characterization presents a similar size distribution of the exosomes with the concentration of 1.12×10^8 particles/μL (Fig. S1A).

For the modification of alkynyl-4-ONE on the exosomes, the aldehyde groups of this molecule reacted with the amino groups on the exosomal proteins to form covalent bonds. Thus, it could be observed that alkynyl-4-ONE-modified exosomes exhibit an increased diameter of 80–110 nm (Fig. 1B) compared with the unmodified exosomes. The analysis by AFM images provides the similar results (Figs. S1B and C), indicating the successful conjugation of alkynyl-4-ONE to the exosomes without destroying the integrity of their membranes.

3.2. Characterization of the aptasensor

To confirm the modification of the GCE, SEM, XRD, Raman and XPS were employed to characterize the rGO/GCE and DenAu/rGO/GCE (Fig. S2). Clearly, the rGO/GCE has a smooth lamellar structure observed from SEM images (Fig. S2A), which could increase the effective area and conductivity of the electrode. Meanwhile, gold deposited on the rGO/GCE presents special three-dimensional dendritic nanostructures with several hundred nanometers in width and ~3 μM in length (Fig. S2B), providing a larger active area for the modification of aptamer. Fig. S2C shows the XRD pattern of GO, rGO and DenAu/rGO. GO (curve a) has a sharp and strong peak at $2\theta = 10.9^\circ$, corresponding to an interlayer spacing of 0.81 nm. rGO (curve b) exhibits a broad diffraction peak located at $2\theta = 24.9^\circ$, and the characteristic peak of GO disappeared, indicating that rGO had been successfully obtained. DenAu/rGO (curve c) shows new characteristic diffraction peaks at $2\theta = 38.6^\circ$, 44.8°, 65.5° and 87.8°, revealing that DenAu was successfully modified on the electrode surface (Ismaili et al., 2011). The Raman spectrum has been presented in Fig. S2D. The G-bond of rGO is shifted to 1584 cm compared to GO (1590 cm, curve a), whereas the D-bond of rGO presents a blue shift from 1345 cm (observed at GO) to 1339 cm. The G-bond and D-bond of DenAu/rGO (curve c) are localized at

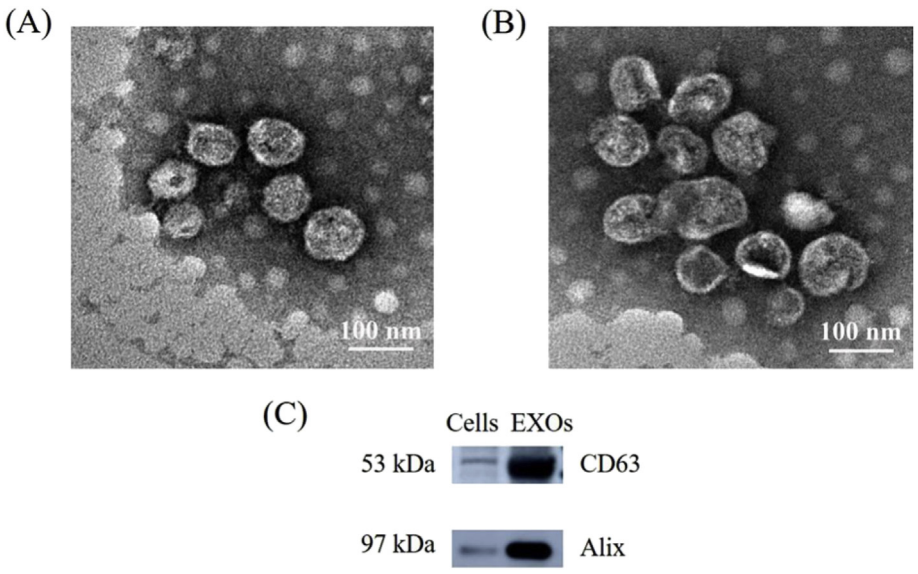

Fig. 1. TEM images of (A) the unmodified exosomes and (B) the modified exosomes with alkynyl-4-ONE, and (C) Western blot analysis for CD63 and Alix protein in the exosomes.

1588 cm and 1350 cm, respectively, showing a moderate red shift compared to rGO (Pocklanova et al., 2016). The XPS spectra have been shown in Figs. S2E–H. GO (Fig. S2E) has 4 main type of carbon bonds: C-C (284.6 eV), C-O (286.7 eV), C=O (287.1 eV) and O-C=O (288.9 eV) (Liu et al., 2013). After electrochemical reduction (Fig. S2F), the absorbance peaks of C-C bond dramatically increase, while the peak intensities of both C-O and C=O sharply decrease. These results indicated that the most of oxygen functional groups on the GO were successfully removed. Figs. S2G and H show the XPS spectra of DenAu/rGO. The C1s peak is basically consistent with rGO, and the Au4f peaks at the binding energies of Au4f7/2 (84.07 eV) and Au4f5/2 (87.75 eV) indicate the formation of the DenAu (Zeng et al., 2012).

The CV and EIS were performed to monitor each immobilization step in 5.0 mM $[Fe(CN)_6]^{3-/4-}$ solution containing 0.1 M KCl. As shown in Fig. 2A, it could be observed that a couple of reversible redox peaks of bare GCE shows a peak potential separation (ΔEp) was approximately 100 mV (curve a). After the deposition of rGO and DenAu on the electrode surface, the current intensity has a significant increase, reflecting an excellent conductivity (curve b), because rGO and DenAu could provide a large active area and thus facilitate fast electron transfer. With the self-assembly of CD63 aptamer on DenAu/rGO/GCE, the current intensity exhibited an obvious reduction (curve c), since the phosphate backbone of aptamers with negative charges inhibited the diffusion of $[Fe(CN)_6]^{3-/4-}$ to the electrode surface (Yan et al., 2012), which reveals that the CD63 aptamer was successfully modified on the electrode. After the blocking with MCH, the current intensity further decreases due to the sealing of the electrode (curve d). When the exosomes were captured on the modified electrode, the negatively charged lipid bilayers and proteins on the surface of exosomes inhibits the diffusion of $[Fe(CN)_6]^{3-/4-}$ to the electrode surface, leading to a sharp decrease in current intensity (curve e). The conjugation of alkynyl-4-ONE to the exosomes by click chemistry and the occurrence of HCR for signal amplification further hinder the electron transfer (curve f). From Fig. 2B, an equivalent circuit was introduced to illustrate the electrical properties of aptasensor with four parameters: the solution resistance (R_s), the charge transfer resistance between the electrode and the solution interface (R_{et}), the double layer capacitance of the electrodes (C_{dl}) and the Warburg impedance (W) (inset of Fig. 2B) (Qiu et al., 2016). R_{et} could be determined by the semicircle diameter of the Nyquist curve (Hou et al., 2014). The EIS results were consistent with that of CVs, both indicating that each immobilization step was successfully fabricated on the electrodes surface.

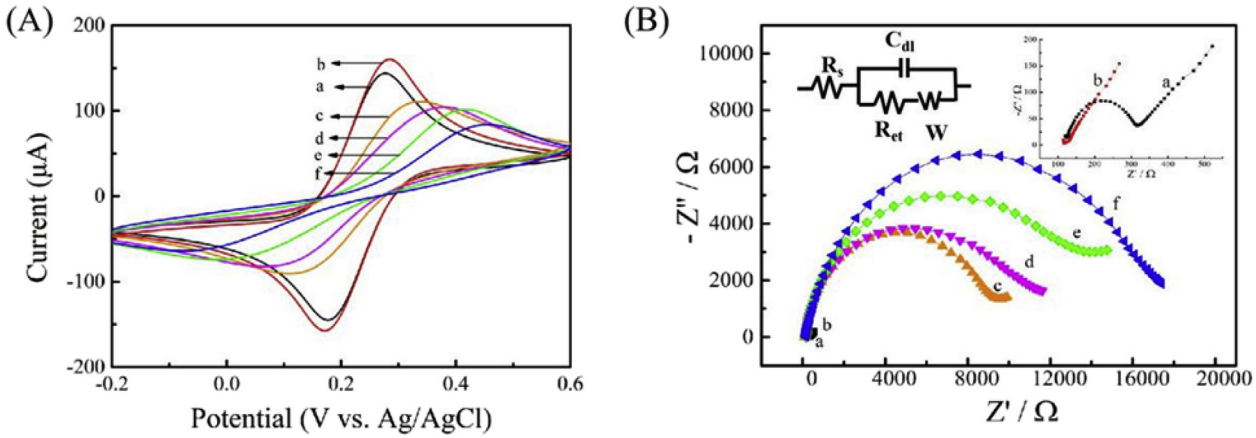

Fig. 2. CV (A) and EIS (B) of different modified GCEs in 0.1 M KCl containing 5.0 mM $[Fe(CN)_6]^{3-/4-}$ solution: bare GCE (a), DenAu/rGO/GCE (b), CD63 aptamer/DenAu/rGO/GCE (c), MCH/CD63 aptamer/DenAu/rGO/GCE (d), exosomes/MCH/CD63 aptamer/DenAu/rGO/GCE (e), and HCR-exosomes/MCH/CD63 aptamer/DenAu/rGO/GCE (f).

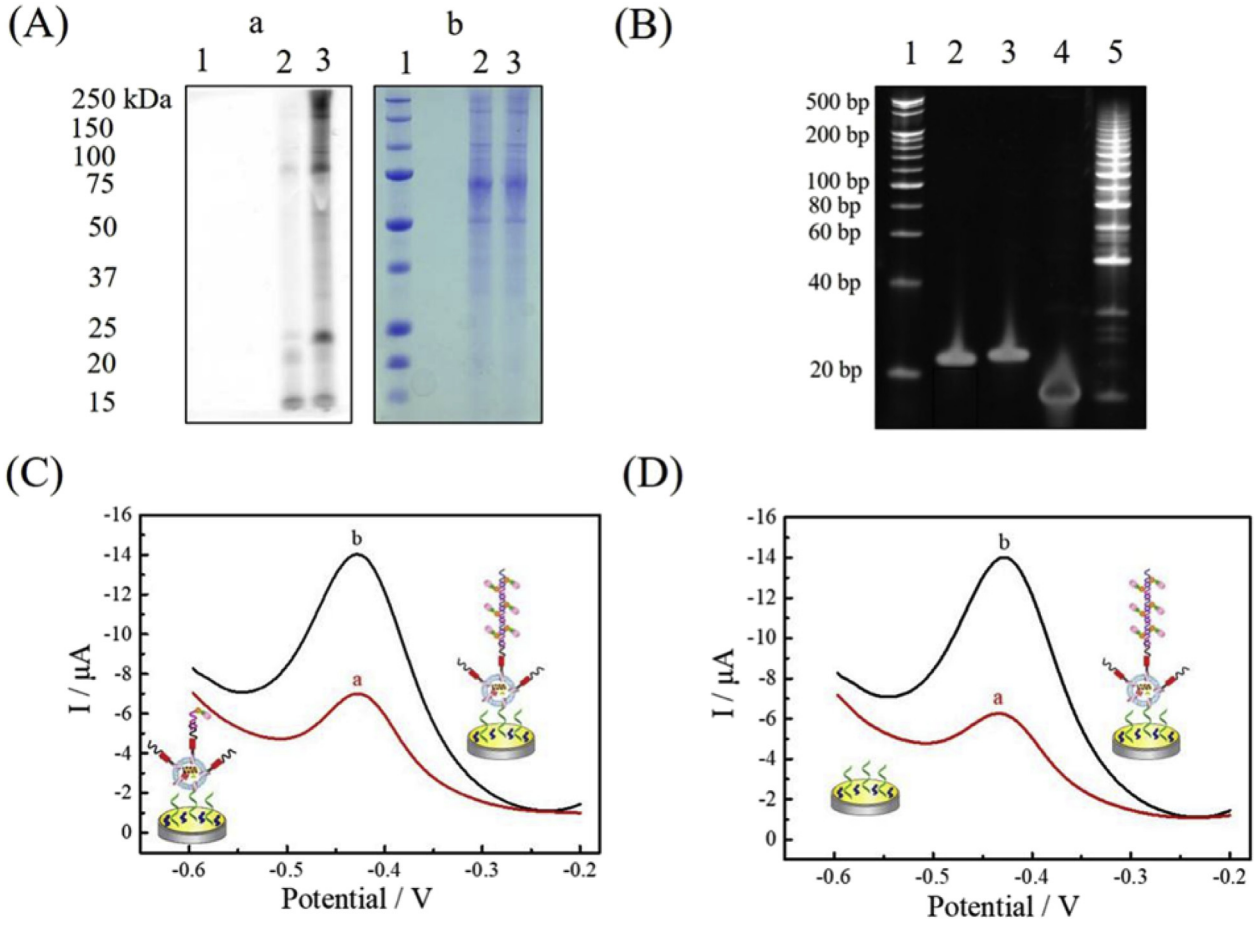

Fig. 3. (A) SDS-PAGE analysis for the click chemistry with (a) and without (b) dyeing by coomassie brilliant blue: protein marker (Lane 1), exosomes treated with 3 μM ssDNA A, $CuSO_4$ and TCEP (Lane 2), and exosomes treated with 5 μM alkynyl-4-ONE, 3 μM ssDNA A, $CuSO_4$ and TCEP (lane 3); (B) urea-PAGE images for the HCR assay: DNA marker (Lane 1), 5.0 μM biotin-H1 (Lane 2), 5.0 μM biotin-H2 (Lane 3), 3.0 μM N_3-anchor (Lane 4), and 3.0 μM N_3-anchor mixed with 5.0 μM biotin-H1 and 5.0 μM biotin-H2 (Lane 5); (C) DPV responses with (a) and without (b) signal amplification by HCR; (D) DPV responses with (a) and without (b) the recognition of exosomes.

SDS-PAGE was employed to verify the performance of click chemistry. Before dyed by coomassie brilliant blue (Fig. 3A (a)), the exosomes treated by the ssDNA A (5-terminal labeled azide and 3-terminal labeled Cy3) solution with alkynyl-4-ONE (Lane 3) had a stronger fluorescence signal compared to the ones treated by the ssDNA A solution without alkynyl-4-ONE (Lane 2). After dyed by coomassie brilliant blue (Fig. 3A (b)), it could be observed that Lane 2 and Lane 3 present almost the consistent bands, showing the same exosome proteins and their concentrations. The results demonstrated the successful modification of alkynyl-4-ONE and the following connection of the N_3-anchor to exosomes by copper (I)–catalyzed click chemistry. The formation of long DNA concatamers by HCR was characterized by urea-PAGE, and the results are shown in Fig. 3B. Clearly, the gel electrophoresis images of biotin-H1 (Lane 2), biotin-H2 (Lane 3) and N_3-anchor (Lanes 4) display only one band at 30 bp, 30 bp and 20 bp, respectively. While, after incubating biotin-H1, biotin-H2 with N_3-anchor at 37 °C for 3 h, the formed long DNA concatamers (Lane 5) exhibits the wide distribution of broad band from 20 bp to 500 bp, revealing that HCR was successful performed.

The effect of signal amplification by HCR was investigated by DPV determination. Fig. 3C indicates that the HCR of biotin-H1 and biotin-H2 generates an obviously amplified DPV signal because the formed long DNA concatemers could capture more HRP. While, in the absence of biotin-H2, each biotin-H1 could only combine with one HRP molecule, leading to a low catalytic efficiency. Fig. 3D displays the responses with and without the exosomes. Clearly, when the exosomes at the concentration of 1.12×10^6 particles/μL were immobilized on the modified electrode, there was a DPV signal approximately 5 times higher than that without the exosomes. All of the results reveal the feasibility of exosome detection with the developed electrochemical aptasensor based on click chemistry and HCR for signal amplification.

3.3. Optimization of the experimental conditions

To obtain the most improved detection sensitivity of tumor exosomes, the main experimental conditions were investigated, including the concentrations of CD63 aptamer, alkynyl-4-ONE, N_3-anchor, biotin-H1 and biotin-H2, the reaction times of alkynyl-4-ONE with exosomes and HCR, and the pH of the detection solution. For the optimization of the CD63 aptamer concentration, the aptamer at different concentrations was immobilized on the DenAu/rGO/GCE. As shown in Fig. S3A, by increasing the concentration of aptamer from 2 μM to 9 μM, the DPV signal gradually increases until it reaches a plateau. Thus, the optimal CD63 aptamer concentration was fixed at 5 μM. The concentration and reaction time of alkynyl-4-ONE with exosomes were key factors for the amount of N_3-anchor combined with exosomes. From Fig. S3B, it could be observed that the reduction current first increases and then remains almost constant in the range of 1–9 μM. Hence, 5 μM was selected as the optimal concentration of alkynyl-4-ONE. The reaction time of alkynyl-4-ONE with exosomes was studied in the range from 30 min to 3 h. The signal significantly increases until 1 h, and then, it hardly changes with the prolongation of the reaction time (Fig. S3C). Hence, 1 h was

selected as the optimal reaction time of alkynyl-4-ONE and exosomes. Fig. S3D shows the effect of the N_3-anchor concentration on the DPV response. Clearly, the DPV signal gradually increases from 1 to 3 μM and the further rising of the concentration doesn't generate an increased current. Therefore, 3 μM N_3-anchor was employed in the following determinations. The important factors influencing the combined quantity of HRP were the concentration of biotin-H1and biotin-H2, and the performation time of HCR. As shown in Fig. S3E, the reduction current first increases with increasing the concentrations of biotin-H1 and biotin-H2 from 1 μM to 5 μM, but as their concentrations increase from 5 μM to 9 μM, the response current hardly changed, suggesting that the long DNA concatemers have reached saturation. Hence, 5 μM was selected as the optimal concentration of biotin-H1 and biotin-H2. From Fig. S3F, it could be observed that with the incubation time of biotin-H1 and biotin-H2 on the modified electrode increasing from 1 h to 5 h, the DPV signal gradually increases until reaching a plateau. Consequently, 3 h was selected as the optimal incubation time. Fig. S3G illustrates the effect of the pH of the detection solution on the catalytic efficiency of HRP. The peak current continuously increases in the pH range of 4–5. While, when the pH value is larger than 5, the peak current dramatically drops, indicating that HRP displays the highest catalytic activity for OPD and H_2O_2 in 0.2 M HAc/NaAc (pH = 5.0) buffer solution.

3.4. Analytical performance of the aptasensor

Under the optimal experimental conditions, the exosomes from MCF-7 cells at different concentrations were determined to investigate the analytical performance of this electrochemical aptasensor. As shown in Fig. 4A, a gradually enhanced DPV signal is presented with increasing concentrations of exosomes, since the larger number of captured exosomes could result in more HRP linked on the electrode. A good linear relationship could be obtained between the DPV signal and the logarithm of the exosome concentration in the range of 1.12×10^2–1.12×10^8 particles/μL (Fig. 4B) with the equation of $\Delta I = -1.0229 \times \lg c - 1.5389$ ($R^2 = 0.9925$), where ΔI represents the difference in the signal with and without the exosomes on the modified electrode under the same conditions, and c represents the concentration of exosomes. The limit of detection (LOD) was calculated as 96 particles/μL, which was lower than most currently reported methods (Table S2), displaying the high potential of this aptasensor in the application of clinic diagnosis.

3.5. Reproducibility and stability

Reproducibility and stability are important parameters for evaluating electrochemical biosensors. To investigate the reproducibility, nine modified electrodes under the same conditions were used to detect the exosomes at the concentration of 2.0×10^6 particles/μL. The relative standard deviation (RSD) of current was 7.6%, reflecting a good reproducibility of the electrochemical biosensor (Fig. S4A). Its stability was investigated by measuring the current signals every 7 days with the storage at 4 °C (Fig. S4B). After 7 days, the signal intensity retained about 97.8% of the initial values. For another 7 days, the current decreased to 91.9%. 21 days later, it had only 88.5% of the initial values, probably due to the reduced activity of HRP under long-term storage. Consequently, this aptasensor can maintain high stability within 14 days.

3.6. Detection of exosomes in human serum

To assess the practical ability of this aptasensor in human serum samples for clinical utility, exosomes derived from a breast cancer patient (P) and a healthy individual (H) were analyzed. In order to evaluate the accuracy of our method, the isolated exosomes were quantified by NTA. As shown in Fig. 5, the concentration of exosome from a breast cancer patient serum was obviously higher than that from healthy individual, which were consistent with the results of NTA. While, it could be observed that lower concentrations were detected by our method, because the value of NTA might be interfered with similarly sized lipoproteins and protein aggregates. To be concluded, this biosensor could be applied to clinical samples, showing high potential in cancer diagnosis.

4. Conclusions

In summary, the biosensor used alkynyl-4-ONE for the nonspecific conjugation of protein on the surface of exosomes, preventing the omission of exosome subpopulations, and took advantage of the high efficiency of click chemistry for the more accurate detection of exosomes. Meanwhile, the strength of HCR was combined for signal amplification, presenting the applicability in the analysis of serum samples. Since the determination of exosomes in this work is based on nonspecific capture, it could enhance the accuracy, and also the sensitivity. The future work will focus on the specific tumor markers on the exosomes for achieving the exosomes-based early diagnosis of tumor.

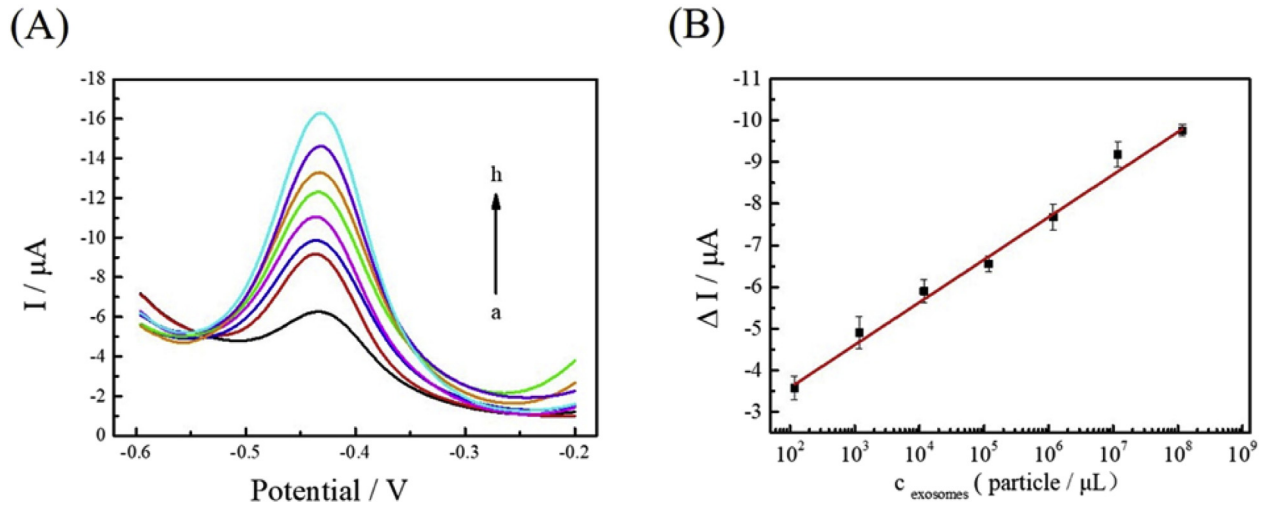

Fig. 4. (A) DPV responses of the electrochemical aptasensor for the exosomes at different concentrations (a–h: 0, 1.12×10^2, 1.12×10^3, 1.12×10^4, 1.12×10^5, 1.12×10^6, 1.12×10^7, and 1.12×10^8 particles/μL, respectively); (B) linear relationship between the electrochemical signal and the logarithm of the exosome concentration. Error bars represent the relative standard deviation of measurements (%RSD ≤7.6%, n = 3).

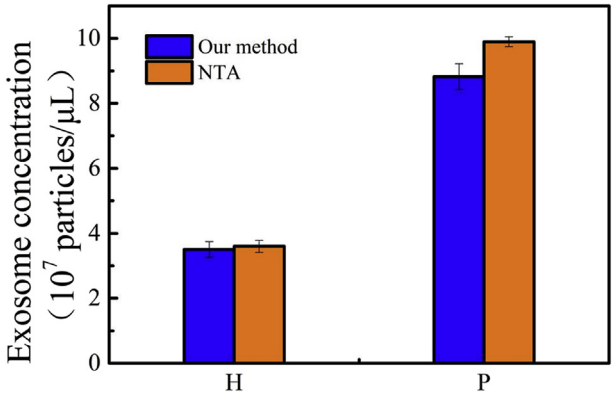

Fig. 5. Comparison of our method and NTA method for the detection of exosomes in serum samples derived from a breast cancer patient (P) and a healthy individual (H). Error bars represent the relative standard deviation of measurements (%RSD ≤ 7.6%, n = 3).

CRediT authorship contribution statement

Yu An: Investigation, Writing - original draft. **Tongyu Jin:** Data curation. **Yuyuan Zhu:** Formal analysis. **Fan Zhang:** Writing - review & editing. **Pingang He:** Writing - review & editing.

Acknowledgments

This work was financially supported by the National Natural Science Foundation of China (Grant No. 21575042).

Appendix A. Supplementary data

Supplementary data to this article can be found online at https://doi.org/10.1016/j.bios.2019.111503.

References

Aluise, C.D., Camarillo, J.M., Shimozu, Y., Galligan, J.J., Rose, K.L., Tallman, K.A., Marnett, L.J., 2015. Chem. Res. Toxicol. 28 (4), 817–827.
Azmi, A.S., Bao, B., Sarkar, F.H., 2013. Cancer. Metast. Rev. 32 (3–4), 623–642.
Boriachek, K., Islam, M.N., Gopalan, V., Lam, A.K., Nguyen, N.T., Shiddiky, M.J.A., 2017. Analyst 142 (12), 2211–2219.
Chen, X., Lan, J., Liu, Y., Li, L., Yan, L., Xia, Y., Wu, F., Li, C., Li, S., Chen, J., 2018. Biosens. Bioelectron. 102, 582–588.
Conlan, R.S., Pisano, S., Oliveira, M.I., Ferrari, M., Pinto, I.M., 2017. Trends Mol. Med. 23 (7), 636–650.
Galligan, J.J., Rose, K.L., Beavers, W.N., Hill, S., Tallman, K.A., Tansey, W.P., Marnett, L.J.J., 2014. Am. Chem. Soc. 36 (34), 11864–11866.
He, F., Liu, H., Guo, X., Yin, B.C., Ye, B.C., 2017. Anal. Chem. 89 (23), 12968–12975.
He, F., Wang, J., Yin, B.C., Ye, B.C., 2018. Anal. Chem. 90 (13), 8072–8079.
Hou, L., Gao, Z.Q., Xu, M.D., Cao, X., Wu, X.P., Chen, G.N., Tang, D.P., 2014. Biosens. Bioelectron. 54, 365–371.
Ismaili, H., Geng, D., Sun, A.X., Kantzas, T.T., Workentin, M.S., 2011. Langmuir 27 (21), 13261–13268.
Jeong, S., Park, J., Pathania, D., Castro, C.M., Weissleder, R., Lee, H., 2016. ACS Nano 10 (2), 1802–1809.
Jin, D., Yang, F., Zhang, Y., Liu, L., Zhou, Y., Wang, F., Zhang, G.J., 2018. Anal. Chem. 90 (24), 14402–14411.
Liang, L., Astruc, D. Coordin, 2011. Chem. Rev. 255 (23–24), 2933–2945.
Liu, Y., Jiao, L., Wu, Q., Zhao, Y., Cao, K., Liu, H., Wang, Y., Yuan, H., 2013. Nanoscale 5 (20), 9562–9567.
Mathivanan, S., Simpson, R.J., 2009. Proteomics 9, 4997–5000.
Moses, J.E., Moorhouse, A.D., 2007. Chem. Soc. Rev. 36 (8), 1249–1262.
Picciolini, S., Gualerzi, A., Vanna, R., Sguassero, A., Gramatica, F., Bedoni, M., Masserini, M., Morasso, C.F., 2018. Anal. Chem. 90 (15), 8873–8880.
Pocklanova, R., Rathi, A.K., Gawande, M.B., Datta, K.K.R., Ranc, V., Cepe, K., Petr, M., Varma, R.S., Kvitek, L., Zboril, R., 2016. J. Mol. Catal. A Chem. 424, 121–127.
Pospichalova, V., Svoboda, J., Dave, Z., Kotrbova, A., Kaiser, K., klemova, D.J., 2015. Extracell. Vesicles 4 (1), 25530.
Qiu, Z.L., Shu, J., Jin, G.X., Xu, M.D., Wei, Q.H., Chen, G.N., Tang, D.P., 2016. Biosens. Bioelectron. 77, 681–686.
Raposo, G., Stoorvogel, W.J., 2013. Cell Biol. 200 (4), 373–383.
Shao, H., Im, H., Castro, C.M., Breakefield, X., Weissleder, R., Lee, H., 2018. Chem. Rev. 118 (4), 1917–1950.
Sharma, S., Rasool, H.I., Palanisamy, V., Mathisen, C., Schmidt, M., Wong, D.T., Gimzewski, J.K., 2010. ACS Nano 4 (4), 1921–1926.
Smyth, T., Petrova, K., Payton, N.M., Persaud, I., Redzic, J.S., Graner, M.W., Jones, P.M., Anchorduquy, T.J., 2014. Bioconjug. Chem. 25 (10), 1777–1784.
Suchorska, W.M., Lach, M.S., 2016. Oncol. Rep. 35 (3), 1237–1244.
Tang, W., Wang, Z., Yu, Zhang, F., He, P., 2018. Anal. Chem. 90 (14), 8337–8344.
Tian, Q., He, C., Liu, G., Zhao, Y., Hui, L., Mu, Y., Tang, R., Luo, Y., Zheng, S., Wang, B., 2018a. Anal. Chem. 90 (11), 6556–6562.
Tian, T., Zhang, H.X., He, C.P., Fan, S., Zhu, Y.L., Qi, C., Huang, N.P., Xiao, Z.D., Lu, Z.H., Tannous, B.A., Gao, J., 2018b. Biomaterials 150, 137–149.
Uttamapinant, C., Tangpeerachaikul, A., Grecian, S., Clarke, S., Singh, U., Slade, P., Gee, K.R., Ting, A.Y., 2012. Angew. Chem. Int. Ed. 51 (24), 5852–5856.
Vestad, B., Llorente, A., Neurauter, A., Phuyal, S., Kierulf, B., Kierulf, P., Skotland, T., Sandvig, K.J., 2017. Extracell. Vesicles 6 (1), 1344087.
Wang, M., Altinoglu, S., Takeda, Y.S., Xu, Q., 2015. PLoS One 10 (11), e0141860.
Xia, Y., Liu, M., Wang, L., Yan, A., He, W., Chen, M., Lan, J., Xu, J., Guan, L., Chen, J., 2017. Biosens. Bioelectron. 92, 8–15.
Yan, M., Zang, D.J., Ge, S.G., Ge, L., Yu, J.H., 2012. Biosens. Bioelectron. 38 (1), 355–361.
Zeng, T., Ma, Y., Niu, H., Cai, Y., 2012. J. Mater. Chem. 22 (35), 18658–18663.
Zhang, H., Freitas, D., Kim, H.S., Lyden, D., 2018. Nat. Cell Biol. 20 (3), 332.
Zhao, L., Liu, W., Xiao, J., Cao, B.W., 2015. Cancer Lett. 356 (2), 339–346.